

# NJC

New Journal of Chemistry

Accepted Manuscript

A journal for new directions in chemistry

This article can be cited before page numbers have been issued, to do this please use: V. Jejurkar, G. Yashwantrao and S. Saha, *New J. Chem.*, 2020, DOI: 10.1039/D0NJ01735C.



This is an Accepted Manuscript, which has been through the Royal Society of Chemistry peer review process and has been accepted for publication.

Accepted Manuscripts are published online shortly after acceptance, before technical editing, formatting and proof reading. Using this free service, authors can make their results available to the community, in citable form, before we publish the edited article. We will replace this Accepted Manuscript with the edited and formatted Advance Article as soon as it is available.

You can find more information about Accepted Manuscripts in the [Information for Authors](#).

Please note that technical editing may introduce minor changes to the text and/or graphics, which may alter content. The journal's standard [Terms & Conditions](#) and the [Ethical guidelines](#) still apply. In no event shall the Royal Society of Chemistry be held responsible for any errors or omissions in this Accepted Manuscript or any consequences arising from the use of any information it contains.

# Tröger's Base Functionalized Recyclable Porous Covalent Organic Polymer (COP) for the Dye Adsorption from Water

Valmik P. Jejurkar,<sup>[a]</sup> Gauravi Yashwantrao,<sup>[a]</sup> and Satyajit Saha\*<sup>[a]</sup>

Cite this: DOI: XXXXXXXXXXXXXXXX

**Abstract:** Protection of the environment from the uprising threats of pollution from several chemical industries in a sustainable way has become the major global challenge. The colored effluents from the textile and dyestuff industries are the major sources of pollution, contaminating the water bodies. Herein, we have synthesized a covalent organic polymer **TBTPACOP** having a V-shaped Tröger's base unit into the framework with the notion that the unique cleft like architecture of TB will infuse porosity and robustness in the amorphous polymeric material. The covalent organic polymer (COP) was used for the adsorption of anionic acid dyes from the aqueous effluent. The equilibrium adsorption capacity ( $q_e$ ) was found to be 188.96 mg/g. The excellent dye adsorption capacity of the COP by adsorbing 95% of the acid dye (Acid Orange II) at room temperature within 70 mins, along with its recyclability up to 4 consecutive cycles, makes **TBTPACOP** an extremely promising material for selective and efficient removal of acid dyes from the aqueous effluent.

## 1. Introduction

There is a severe rise in the global concern for protecting the environment from the uprising threats of pollutions created from several chemical industries.<sup>1-3</sup> Textile and dyestuff industries are considered as the prime polluters due to their discharge of colored effluents into the hydrosphere. The discharge of colored effluents into the environment gives an undesirable color to the water even at a very low concentration, thereby reducing sunlight penetrability, causing serious harm to marine life. These colored effluents are normally water-soluble organic dyes which are non-oxidizable as well as non-degradable under light or heat. Dye contaminated water even raises the threat for several mutagenic and teratogenic diseases by incorporating the toxic dye molecules into the food chain.<sup>4-7</sup> Hence, the efficient removal of toxic dyes before the effluent is discharged into the environment throws a major challenge towards sustainable development.

Several methods have been developed for the removal of dye from the dye contaminated effluents. However, the development of rapid cost-effective removal of a low level of dye contaminants is always challenging.<sup>8-12</sup> Decontamination techniques by coagulation, advanced oxidation process, membrane separation techniques, electrochemical oxidative methods along with the adsorption by activated charcoal, multi-walled carbon nanotubes, cedar sawdust, brick, graphene-based materials, chitin, fly ash, silica gels are existing but there are persistent efforts towards the understanding the mechanism of dye removal and development of newer methods as well as designing novel materials for the dye removal from the effluent.<sup>13-36</sup>

Recently, covalent-organic polymers (COPs), analogous to the covalent organic framework (COF), have stimulated extensive interest due to their high adsorption capability, large surface area, high porosity, chemical tunability, enhanced stability as well as easy synthetic accessibility.<sup>20-25</sup> Covalent organic polymers (COPs) belongs to a group of porous organic materials constructed by linking several organic building blocks via covalent bond formation, having applications in drug delivery,

separation techniques, chemical sensors, gas storage, catalysis, optoelectronics, energy storage, as well as biomedical products, etc.<sup>20-70</sup> Owing to their large surface area and impressive porosity, COP might adsorb organic molecules thereby making them an ideal contender for the removal of dyes from the effluent. However, the exploration of porous organic materials (POMs) for water treatment is still at its infancy and it is, therefore, necessary to rationally design COP to extend their applications towards water treatment.

The properties of a COP are highly dependent on the morphology of the COP as well as the constituting monomeric linker units, which can be functionally tuned to improve the corresponding chemical property. Several organic linkers with diverse functionalities were explored to synthesize COPs intended for numerous applications. Depending on the requirement of the tailor-made geometries of the COP with high structural rigidity, the availability of the building blocks is still limited. Herein, we have tried to introduce novel building block bearing V-shaped Tröger's base (TB) unit into the framework with the intention that this unique V-shaped molecule will provide structural rigidity and incorporate a porous hydrophobic cavity within the polymer.

Tröger's base, although discovered in 1887, its potential was only realized when it was first used as a chiral host material. Since then, this unique scaffold has gained tremendous popularity and incorporation of Tröger's base, possessing two nitrogen centers within any framework, is known to induce the material towards molecular recognition through non-covalent supramolecular interaction, as well as impart catalytic properties, among several other features.<sup>71-94</sup> Polymers decorated with Tröger's base have been extensively employed in generating membrane material for gas separations. However, to the best of our knowledge, there are no reports of Tröger's-based porous polymer networks studied in the context of adsorbent materials for the removal of organic dyes.

So, in order to obtain the porous material with the desirable property, our idea was to exploit the V-shape core of the TB to construct a covalent organic polymer by chemically linking the C2 symmetric rigid TB with a C3-symmetric core via forming a covalent bond between them (Fig. 1). The architecture of COP depends upon the geometry of linkers present in an altered fashion and the proposed geometry of the COP is presented in Fig. 1. This strategy will feature the unique cleft of Tröger's base in the covalent organic polymer to provide chemical and thermal stability with a potential hydrophobic surface and opportunity to tweak the functionality by tuning the surface morphology. The nitrogen atoms make the pore of the framework polar, suitable for adsorbing the substrate dye molecules through some non-covalent interaction.

As part of our contribution towards sustainable development program,<sup>95-97</sup> the present work describes the design and synthesis of an imine linked COP, **TBTPACOP** consisting of Tröger's base linker and its application towards acid dye removal from the aqueous effluent. The solvothermal reaction between the two reacting components, one

[a] Valmik P. Jejurkar, Gauravi Yashwantrao and Dr. Satyajit Saha

Department of Dyestuff Technology,  
Institute of Chemical Technology,  
Mumbai-400019, India

E-mail: [ss.saha@ictmumbai.edu.in](mailto:ss.saha@ictmumbai.edu.in)

ORCID Satyajit Saha: 0000-0003-0407-7251

Supporting information for this article is available on the www. under www.

The synthetic procedures and the <sup>1</sup>H and <sup>13</sup>C NMR of all the intermediates.

bearing a C2-symmetric dialdehyde and the other a C3-symmetric tris-amine, yielded the mesoporous **TBTACOP** in the form of black powder.

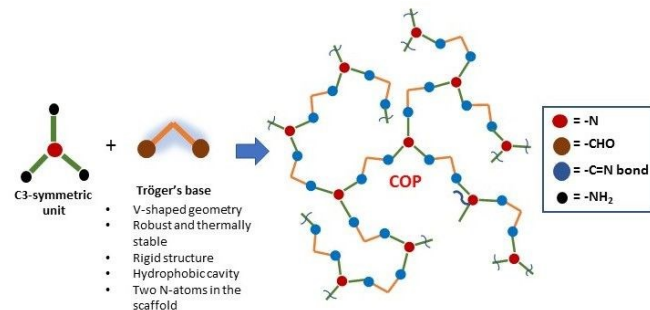
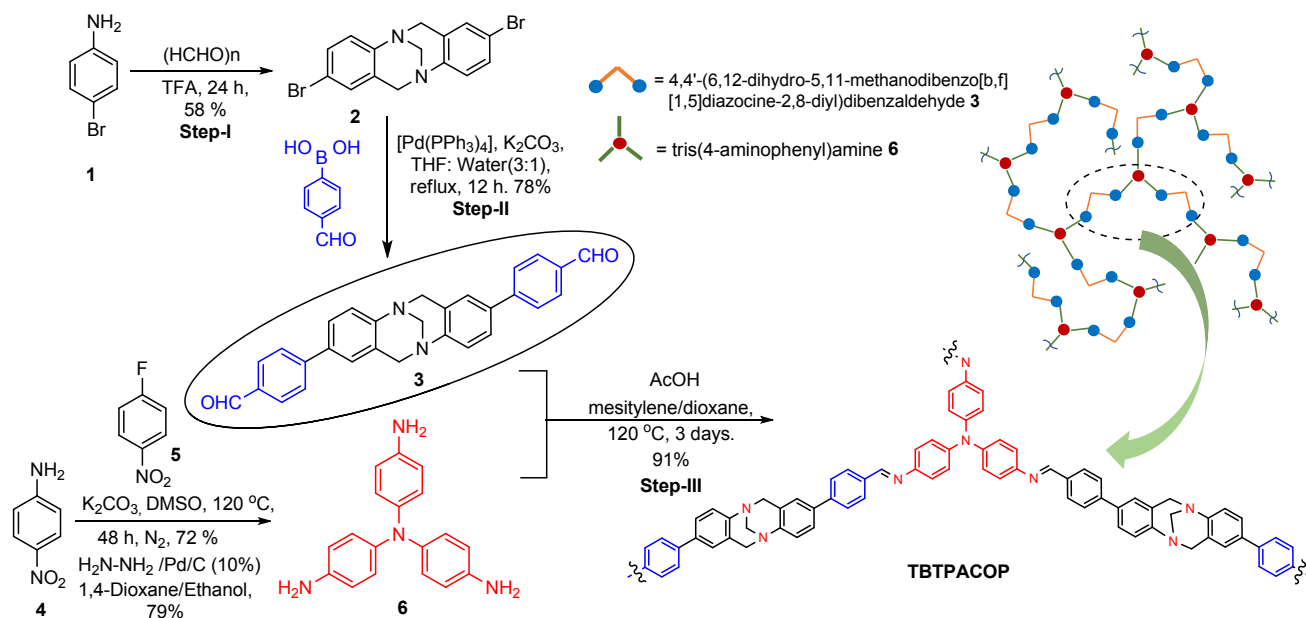


**Fig. 1.** The proposed design strategy for the construction of Tröger's base incorporated COP.

The amorphous nature of **TBTACOP** was confirmed by powder X-ray diffraction (PXRD) pattern which was then structurally and morphologically characterized by several analytical techniques like FT-infrared spectroscopy, solid-state  $^{13}\text{C}$  NMR, SEM, and 3D laser confocal microscopy and nitrogen adsorption isotherms. Dye adsorption kinetics have also been studied. The thermogravimetric analysis revealed the high thermal stability of the COP having a surface area of  $126\text{ m}^2\text{g}^{-1}$  obtained from the BET surface area analysis. **TBTACOP** exhibited superior adsorption of Acid Orange II dye achieving excellent adsorption capability by adsorbing 94% of the acid dye within 70 mins at room temperature with the advantage of recyclability up to 4 cycles. The adsorption propensity of porous **TBTACOP** was selectively observed for acid dyes over other classes of dyes suggesting selective dye adsorption based on H-bonding interaction as well as size-dependent separation.

## 2. Results and Discussion



**Scheme 1.** Synthetic scheme for the preparation of **TBTACOP**.

### 2.3. FT-IR and $^{13}\text{C}$ NMR Analysis

The infrared spectra were recorded on a Jasco (FT-IR-4100) spectrophotometer. The infrared analysis confirmed the bonding and structural features of **TBTPACOP**. The comparison of the infrared spectra (Fig. 2) of **TBTPACOP** (black line) with TPA (blue line), and TBBA (red line) confirms the disappearance of the  $-\text{NH}_2$  and  $-\text{CHO}$  peak and appearance of a  $-\text{C}=\text{N}$  peak. The absorption bands at  $3350\text{--}3450\text{ cm}^{-1}$  and  $1610\text{ cm}^{-1}$  attributes to the corresponding stretching frequencies of  $-\text{N}-\text{H}$  of  $\text{NH}_2$  in TPA **6** whereas the peak appearing at  $1710\text{ cm}^{-1}$  represents the  $-\text{C}=\text{O}$  stretching of the  $-\text{CHO}$  of TBBA **3**. Very weak peaks around  $2700\text{--}2800\text{ cm}^{-1}$  appeared due to the aldehydic  $-\text{C}-\text{H}$  stretching. Thus, when compared to the IR spectra of **3** and **6**, the intensities and the positions of the peaks appearing for **TBTPACOP** have shifted indicating a change in the chemical environment of those bonds. In peak appearing at  $1645\text{ cm}^{-1}$  in the FT-IR spectra of **TBTPACOP** (Fig. 2), confirms the presence of  $-\text{C}=\text{N}$  along with the absence of  $-\text{CHO}$  and  $-\text{NH}_2$  peak.

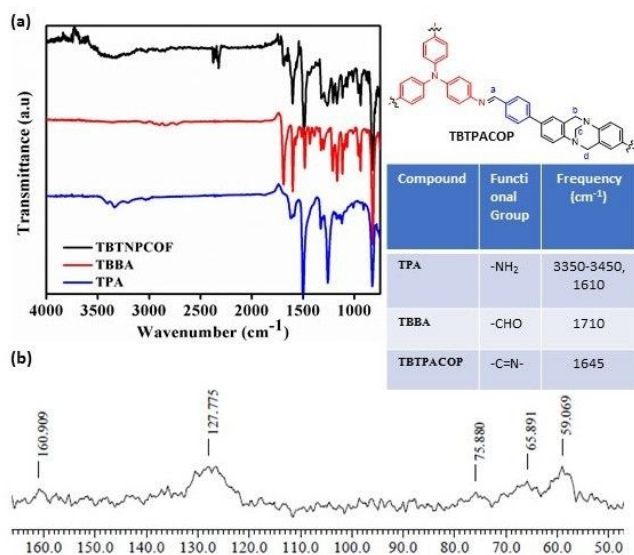


Fig. 2. Characterization of **TBTPACOP** by (a) FT-IR and (b) solid-state  $^{13}\text{C}$  NMR spectroscopy.

The  $^{13}\text{C}$  (CP-MAS) NMR spectral data confirmed the incorporation of TB in the chemical structure of the **TBTPACOP**. The signals appearing at the aliphatic region of the NMR spectrum at  $59.07$ ,  $65.89$ , and  $75.80\text{ ppm}$  correspond to the three  $-\text{CH}_2$ -protons of the Tröger's base linker **3**. The peak appearing at  $160.91\text{ ppm}$  belongs to the newly formed imine carbon in the polymer **TBTPACOP** and the peaks appearing in the region  $122$  to  $140\text{ ppm}$ , belongs to the aromatic carbons of the polymer.

### 2.4. Thermogravimetric Analyses (TGA)

TGA analysis was performed on a TGA4000 Perkin-Elmer instrument under  $\text{N}_2$  atmosphere at a heating rate of  $10\text{ }^\circ\text{C}/\text{min}$ . **TBTPACOP** exhibited high thermal stability up to  $460\text{ }^\circ\text{C}$ , as revealed from the TGA profile, and it retained about 90% of its weight up to  $460\text{ }^\circ\text{C}$  and above  $600\text{ }^\circ\text{C}$  retained 70% of its weight (Fig. 3a). The marginal weight loss observed below  $200\text{ }^\circ\text{C}$  was probably due to the release of the moisture trapped inside the polymeric material. The simultaneous thermal stability of **TBTPACOP** was also analyzed by differential scanning calorimetry (DSC) under a nitrogen atmosphere (Fig. 3a, inset). As represented in the

*New. J. Chem.*

thermogram, **TBTPACOP** exhibited an exothermic glass transition temperature at  $480\text{ }^\circ\text{C}$ , indicating its high thermal stability.

### 2.5. Powder XRD

The powder X-ray diffraction pattern of the synthesized **TBTPACOP** was analyzed on the Bruker D8 Advance X-ray diffractometer with  $\text{CuK}\alpha$  radiation ( $1.5406\text{ \AA}$ ). The analysis of the powder XRD pattern of the **TBTPACOP** at room temperature revealed a broad peak having  $2\theta$  value  $21^\circ$  suggesting amorphous packing of the polymeric network (Fig. 3b, black line). The corresponding d-spacing (100 planes) calculated from Bragg's equation ( $n\lambda = 2d\sin\theta$ ) is  $0.42\text{ nm}$ .<sup>98</sup> This amorphous nature of the COP could be attributed due to the incorporation of strained linkers within the framework. The combination of V-shaped Tröger's base derived dialdehyde **3** and the tris amine **6** will geometrically not allow the formation of hexagonal network formation thereby resulting in the formation of amorphous polymer with broad diffraction peaks quite contrary to the crystalline COFs reported in the literature.

### 2.6. Effect of Organic Solvents/Alkali/Acid/Temperature on The Stability of the TBTPACOP

The chemical stability of **TBTPACOP** was also probed by immersing **TBTPACOP** for 1h in organic solvents like ethyl acetate and THF as well as in 2N HCl and 2N NaOH solution and analyzing their powder XRD profile after filtration and drying (Fig. 3b). The complete retention of the peak positions in the PXRD patterns along with the conservation of the amorphous nature clarifies the good resistance of **TBTPACOP** under different conditions. The **TBTPACOP** when subjected to heat treatment at  $100\text{ }^\circ\text{C}$  and  $150\text{ }^\circ\text{C}$  for 1 h, retained the PXRD profile without any deviation (Fig. 3b). The unchanged powder XRD profile features the inertness of the **TBTPACOP** framework under different pH, temperature, in aqueous as well as in organic solvents signifying the robustness of the polymeric framework.

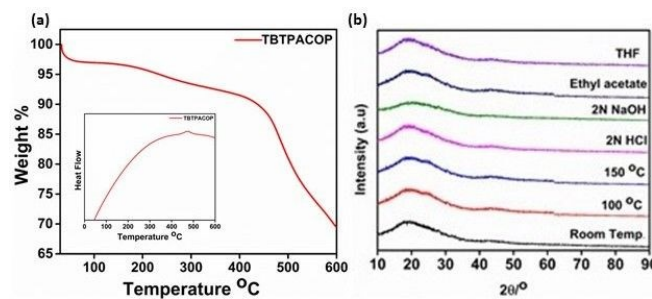


Fig. 3. (a) TGA-DSC thermogram of **TBTPACOP** (b) The powder X-ray diffraction pattern of **TBTPACOP** treated under different conditions.

### 2.7. Scanning Electron Microscopy (SEM) Images

The field emission scanning electron microscopy (FE-SEM) provided the deep insight into the morphological information of **TBTPACOP** (Fig. 4). The synthesized **TBTPACOP** was ultrasonicated in distilled acetone for 10 mins and dried under a high vacuum for 48 h to remove any volatile solvent impurities. The amorphous powder of **TBTPACOP** was then mounted on the stubs using double-sided vacuum compatible carbon tape and analyzed. The SEM images revealed the near-spherical morphology of **TBTPACOP**. These observations indicate that the polymerization through the covalent imine bond formation across the

structure has led to a uniform morphology with a certain degree of structural regularity. As represented in Fig. 4, **TBTPACOP** exhibited porous nature, which might facilitate the adsorption process for the removal of dyes from the effluent.

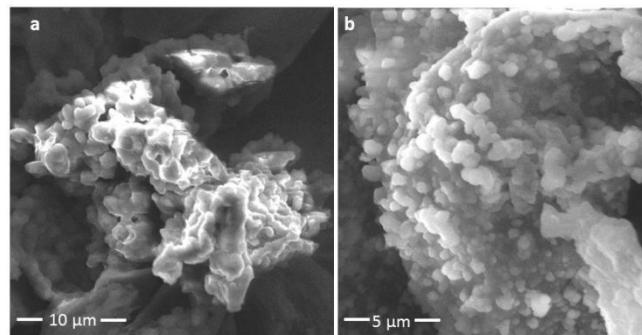


Fig. 4. Field emission scanning electron microscopy (FE-SEM) of **TBTPACOP**.

### 2.8. 3D Laser Confocal Scanning Microscopy

The surface analysis of the covalent organic polymer **TBTPACOP** was done using a ZEISS LSM 900 confocal laser scanning microscope.<sup>99</sup> LSM 900 enables accurate, 3D-imaging, and information about the surface properties of nanomaterials, polymers, metals, and semiconductors. The 3D image of the **TBTPACOP** coated on the surface of a clean glass plate is represented in Fig. 5. The synthesized **TBTPACOP** was ultrasonicated in acetone for 10 mins and dried then under a high vacuum for 48 h to remove volatile solvent impurities. The amorphous powder of **TBTPACOP** was then mounted on the glass plate using double-sided vacuum compatible carbon tape and analyzed by LEXT OLS5000 3D measuring laser microscope.<sup>99</sup> The spherical morphology is evident through the fluorescence imaging of the polymer.

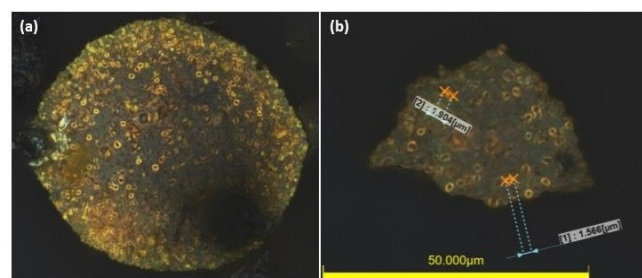


Fig. 5. (a) 3D laser confocal scanning microscopic image of **TBTPACOP** coated on the surface of a glass plate (b) average pore diameter calculation.

### 2.9. BET Surface Area and Porosity Measurement

In order to evaluate the porosity and surface area parameters of **TBTPACOP**, nitrogen adsorption-desorption analysis were performed on Quantachrome Autosorb equipment in 9 mm w/o rod cell at 77 K. Prior to the sorption experiment, the **TBTPACOP** was degassed at 100 °C for 24 h. Ads shown in the Fig. 6, the adsorption isotherm of **TBTPACOP** exhibited a pattern closely related to the Type IV isotherm according to

*New. J. Chem.*

the IUPAC classification and displays a steep nitrogen uptake at relatively low pressure confirming the mesoporous nature of the material (Fig. 6a). From the BET isotherms of **TBTPACOP**, the surface area was found to be 126 m<sup>2</sup>g<sup>-1</sup>. Pore size distribution plot of **TBTPACOP** (Figure 6b) displayed a mean pore width of 6.309 nm and pore volume of 0.199 cm<sup>3</sup>g<sup>-1</sup> further validating the mesoporous nature of the covalent polymer.<sup>100</sup>

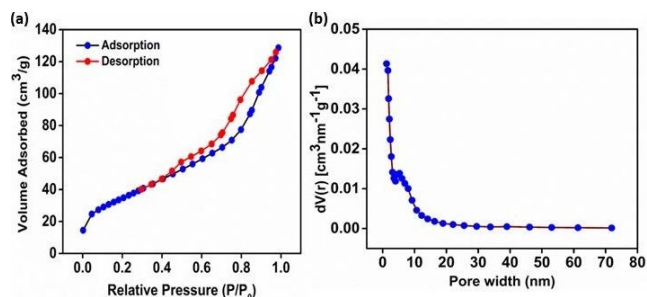


Fig. 6. (a) N<sub>2</sub> Adsorption and desorption isotherm of **TBTPACOP** and (b) pore size distribution plot of **TBTPACOP** by Barret-Joyner-Halenda (BJH) method.

### 2.10. Contact Angle Measurement and Surface Roughness Assessment

Wettability is a much desirable property and can have several applications that demand hydrophobic surfaces. The surface property of the polymeric materials is generally an attribute of the nature of the individual organic linkers or can be modified by external treatment. However, controlling the surface wettability of COP has always been a challenging task. So, to ascertain the surface wettability of the **TBTPACOP**, the contact angle between the water droplet and the polymer surface was measured using ACAM D2A Contact angle meter. The measurement was done by placing a water droplet on the surface of the clean glass surface coated with **TBTPACOP** and recording the corresponding angle. The contact angle was observed to be 133.99° indicating the hydrophobic nature of **TBTPACOP**, Fig. 7. The hydrophobic nature of **TBTPACOP** can be reasoned due to the presence of a TB scaffold at the periphery of the polymeric material.

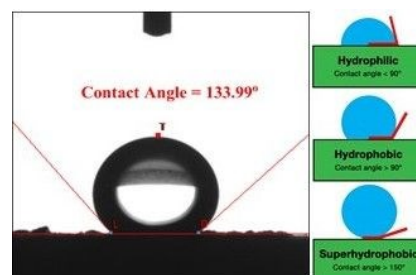


Figure 7. Contact angle measurement displaying the contact point of water over the surface of **TBTPACOP**.

Several industrial applications of organic polymers demand hydrophobic surface along with the information about the surface irregularities. Since the surface structure also influences the function of many polymeric materials, hence the quantification of the surface roughness of the covalent organic polymeric material **TBTPACOP** will help us to assess the

material by height, depth, and interval. The covalent organic polymer **TBTACOP** was coated on a clean glass surface and the 3D topographical images were recorded by ZEISS LSM 900 confocal laser scanning microscope to identify the porosity of the polymeric material. Fig. 8 represents the 3D profiles of the surface of **TBTACOP** and average surface roughness providing a visual representation of the surface topology in the form of patches of crest and troughs. The topological analysis reveals the porous nature of the **TBTACOP**. A representative crest measuring 16.126  $\mu\text{m}$  in length was considered where the height profile was analyzed. It was observed that the surface roughness ranges from -5  $\mu\text{m}$  to 5  $\mu\text{m}$  across the calculated region.

According to the Wenzel theory, surface roughness has a close relationship with the hydrophobicity of the material.<sup>92</sup> A rough surface with a lot of porosity will have an abundance of air pockets located in the grooves. With several air pockets throughout the surface, the trapped air within those pockets will provide air cushioning to the water droplet over it and would prevent the water from further penetrating the grooves. Therefore, the less solid area will be wetted by water, resulting in better hydrophobicity for the rough surfaces of the polymeric material.

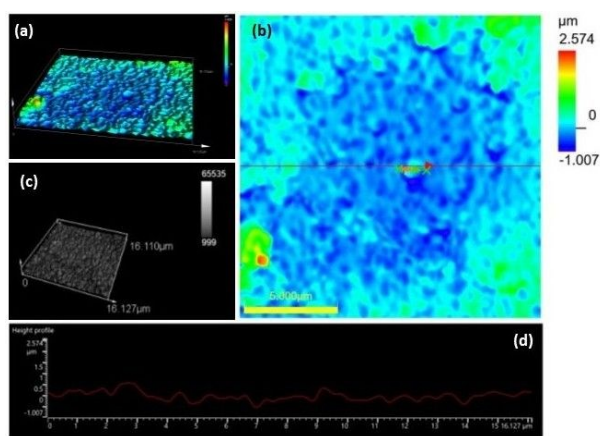


Fig. 8. Color-coded height map of **TBTACOP** by 3D confocal scanning microscopic technique.

### 2.11. Dye Adsorption Study

Efficacy of dye adsorption by **TBTACOP** from the aqueous effluent was tested using Acid orange II (**D1**). Acid orange II (**D1**) is an anionic azo dye having a reddish-yellow color. According to the NFPA and HMIS rating, Acid orange II (**D1**) is considered as a grade 2 hazardous chemical that can cause respiratory tract irritation as well as causes eyes and skin irritation and can also penetrate through the skin. Before studying the adsorption kinetics, to understand the effect of ultrasonication on dye degradation, we sonicated the dye (**D1**) contaminated effluent for 10 mins. There was hardly any observable change in the absorption maxima (483 nm) intensity implying the zero impact of sonication on the degradation of the dye (Fig. 9). Thereafter 1 mg of the **TBTACOP** was added to the 10 ml of the aqueous dye effluent ( $1 \times 10^{-3}$  M) and sonicated for 5 mins. The subsequent spectrophotometric analysis revealed a 56% reduction in the absorption intensity pointing out the involvement of **TBTACOP** in the dye adsorption process (Fig. 9). Further, the adsorption kinetics of the dye was investigated by adding 5 mg of **TBTACOP** to the 10 mL of the effluent containing 0.001 gm of Acid orange II (**D1**). After ultrasonication for 5 mins, the effluent was kept without disturbing.

*New. J. Chem.*

**TBTACOP** was then filtered out and the filtrate was analyzed spectrophotometrically, (Fig. 9). The process was continued until a visually clear effluent was observed. The spectrophotometric analysis of the filtered effluents revealed that there was a gradual reduction of the absorption maxima over time and 95% removal of dye was achieved when stored over **TBTACOP** for 70 mins at room temperature (Fig. 9d). Beyond 70 mins, no notable change was observed. The dye adsorption kinetics of the **TBTACOP** was also visualized by observing the color changes of the aqueous effluent over time (Fig. 9c).

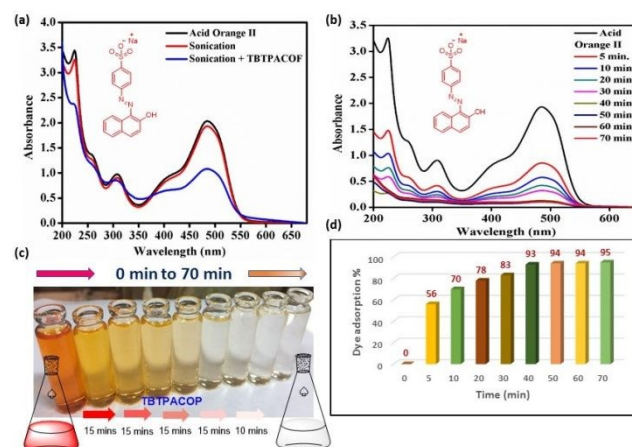


Fig. 9. (a) UV-vis spectral change due to the adsorption of Acid orange II (**D1**) by **TBTACOP** under different conditions (b) UV-vis spectral change due to the adsorption of Acid orange II by **TBTACOP** at different time intervals (c) Visual change of the effluent color due to the Acid orange II adsorption by **TBTACOP** from the aqueous effluent at different time interval (d) Graphical plot of the dye adsorption % over time by the polymer **TBTACOP**.

To further investigate the dye adsorption kinetics, the adsorption of Acid orange II (**D1**) by **TBTACOP** was investigated at different time intervals. The equilibrium adsorption capacity ( $q_e$ ) towards Acid orange II dye was calculated by UV-Vis spectroscopy at different time intervals ( $t$ ) taking 100 ppm initial aqueous solution of **D1** with 5 mg **TBTACOP**. The effect of contact time ( $t = 0, 5, 10, 20, 30, 40, 50, 60,$  and  $70$  min) and the adsorption of Acid orange II (**D1**) by **TBTACOP** is presented in Fig. 10. As expected, the amount of **D1** adsorbed by **TBTACOP** enhanced with increasing contact time. As observed, the adsorption capability of **TBTACOP** increased rapidly initially, then gradually became slow and reached an adsorption equilibrium when no further improvement in the adsorption process was noticed.

The equilibrium adsorption capacity of the Acid orange II (**D1**) by the **TBTACOP** was evaluated according to the equation provided below:

$$q_e = (C_i - C_e) V / W$$

Where  $C_i$  and  $C_e$  are initial and equilibrium concentrations (mg/L) of Acid Orange II (**D1**), respectively,  $V$  is the volume of Acid Orange II (**D1**) solution ( $10 \times 10^{-3}$  L),  $W$  is the amount of **TBTACOP** ( $5 \times 10^{-3}$  g) and the equilibrium concentration = 5.52 mg/L. The equilibrium adsorption capacity ( $q_e$ ) calculated was found to be 188.96 mg/g. The kinetics studies were performed to evaluate the adsorption kinetics of **TBTACOP** towards dye Acid Orange II (**D1**).

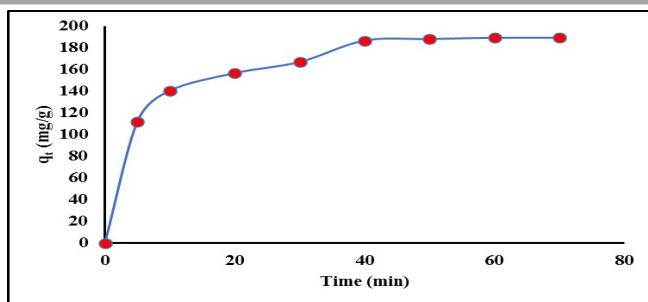


Fig. 10. Graphical plot of adsorption capacity ( $q_t$ ) over time.

Pseudo-first order and pseudo-second order kinetic models were used to investigate the adsorption kinetic properties of **TBTACOP** over Acid Orange II (**D1**). The two different adsorption models can be expressed by equations (1) and (2) after definite integration, by applying the initial conditions  $q_t = 0$  at  $t = 0$  and  $q_t = q_t$  at  $t = t$ .

$$\log(q_e - q_t) = \log q_e - (k_1/2.303) t \quad \text{.....eq.1}$$

$$t/q_t = (1/(k_2 \times (q_e)^2) + (t/q_e) \quad \text{.....eq.2}$$

where,  $q_e$  and  $q_t$  ( $\text{mg g}^{-1}$ ) are the amounts of organic dyes adsorbed per gram of adsorbents at adsorption equilibrium and each time  $t$  (min), respectively.

$k_1$  ( $\text{min}^{-1}$ ) and  $k_2$  ( $\text{mg g}^{-1} \text{min}^{-1}$ ) represent pseudo-first order and pseudo-second-order rate constant. The curve fitting plots of Acid Orange II (**D1**) adsorbed onto **TBTACOP** for both pseudo first order and pseudo second order kinetics are exhibited in Fig. 11 A and B respectively. All the kinetic parameters are listed in Table 1.

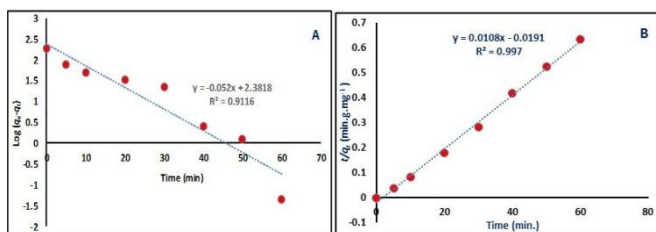


Fig. 11. (A) Pseudo-first order kinetics plot (B) Pseudo-second-order kinetics plot.

**Table 1:** The pseudo-first order and pseudo-second-order rate constants with correlation constants ( $R^2$ ) of Acid Orange II over **TBTACOP** at 100 ppm.

$C_0$	Pseudo-first order model		Pseudo-second order model	
	$k_1$ ( $\text{min}^{-1}$ )	$R^2$	$k_2$ ( $\text{mg g}^{-1} \text{min}^{-1}$ )	$R^2$
100 ppm	0.2474	0.9116	$3.86605 \times 10^{-4}$	0.997

The results revealed that the dye adsorption process fits well with the pseudo second order model over the pseudo first order kinetic model because of the superior linear correlation coefficient ( $R^2 = 0.997$ ) observed as compared to the linear correlation coefficient value ( $R^2 = 0.9116$ ) obtained for pseudo first order model. The pseudo-second-order rate constant  $k_2$  ( $\text{g mg}^{-1} \text{min}^{-1}$ ) and the adsorbed amount of dye at the equilibrium of  $q_e$  ( $\text{mg g}^{-1}$ ) can be obtained from the intercept and slope of

New. J. Chem.

Fig 11 (B). The rate constant  $k_2$  for **TBTACOP** was found to be  $3.866 \times 10^{-4} \text{ mg g}^{-1} \text{min}^{-1}$ . Moreover, the pseudo-second order kinetic model assumes that the mode of adsorption is mainly via chemisorption which might include electron transfer or electron sharing between the adsorbent and adsorbate.

### 2.12. Recyclability Study

Next, we studied the recyclability of **TBTACOP** by filtering and reusing the same polymeric material for the dye adsorption (see Fig. S1, supporting information). It was observed that **TBTACOP** indeed could be recycled efficiently for the dye adsorption process however, the dye adsorption capability of **TBTACOP** gradually reduced from 94% to 70% over the four cycles (Fig. 12). The reduction in the dye adsorption efficiency beyond the 4th cycle could be because of the physical loss of the material.

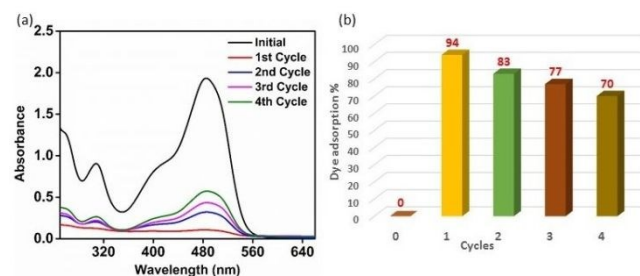


Fig. 12. (a) Recyclability study of **TBTACOP** for the removal of Acid orange II from aqueous effluent (b) Graphical plot of the dye adsorption % over different cycles.

### 2.13. Selective Dye Adsorption Study

Next, we decided to evaluate the ability of **TBTACOP** to adsorb other classes of dyes like direct, basic, and reactive dyes to understand the dye adsorption mechanism. For that purpose, we have selected the following five dyes: Acid Orange II (**D1**), Acid Red 54 (**D2**), Basic Rhodamine B (**D3**), Procion green (**D4**), Direct Turquoise Blue (**D5**), (see Fig. S2, supporting information). Dyes **D1**, **D2**, **D4** are colorants containing azo chromophore whereas **D3** and **D5** are basic triarylmethine dye and Cu-phthalocyanine based direct dye, respectively. The presence of one or multiple sodium sulfonate groups in **D1**, **D2**, **D4**, and **D5** are responsible for the water solubility of these dyes. However, **D3** is devoid of any sulfonic acid group but the positively charged quaternary nitrogen in **D3** accounts for its water solubility. **D1** contains one sodium sulfonate group whereas **D2**, **D5** consisting of two sodium sulfonate groups and, **D4** has six sodium sulfonate groups. **D4** is a reactive dye with a relatively bigger structure and **D5** is a Cu-phthalocyanine based direct dye-containing two sodium sulfonate group. The dye **D3** is a cationic basic dye whereas all other dyes **D1**, **D2**, **D4**, and **D5** are anionic dyes. All these dyes being water-soluble although with different charges and sizes will be a good contender to understand the mechanism of dye adsorption. The dye adsorption kinetics were studied to understand the mode of action as well as the efficacy of **TBTACOP** towards different classes of dyes (Fig. 12). The absorption spectra of all the dyes **D1-D5** before and after the treatment with **TBTACOP** for 70 mins is represented in Fig. S3 (see supporting information). Analysis of the absorption spectra reveals that **D1** and **D2** were effectively adsorbed within 70 mins whereas dyes **D3-D5** were absorbed only in the range of 22-45% by the **TBTACOP**, (Fig. 13).

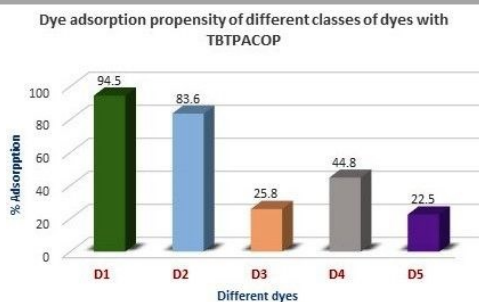


Fig. 13. Study of different dye adsorption capability of TBTPACOP.

The tendency of the acid dyes **D1** and **D2** to get adsorbed easily compared to the dyes **D3–D5** could be due to the presence of OH and NH<sub>2</sub> groups in the structure that can interact with the polar nitrogen atoms of the polymer TBTPACOP via hydrogen bonding. Although dyes **D3** and **D4** have polar -COOH and -NH- groups but size sieving due to their relatively bigger structure could be the probable reason for their poor adsorptivity compared to **D1** and **D2**. Moreover, the electrostatic interaction between the TBTPACOP and the dye molecules as the possible mode of adsorption could be ruled out due to the absence of any ionic centers or surface charge in the TBTPACOP, which accounts for the poor adsorptivity of **D5**, apart from the relatively bigger size of **D5**, being the other reason. However, both **D1** and **D2** having a comparable size, the higher % adsorption of **D1** compared to **D2** could be due to the presence of two sodium sulfonate groups in **D2** which makes it more soluble in water than **D1** and making it slightly more difficult to get adsorbed compared to **D1**. Therefore, size sieving and hydrogen bond interaction could be the possible modes of adsorption of the acid dyes from the aqueous effluent. Moreover, slightly better adsorption rate of **D4** compared to **D3** and **D5** may be probably due to the more number of hydrogen bond donor groups in **D4**. Further, we studied the influence of other dyes on the adsorption capability of the TBTPACOP. An equimolar mixture of **D1** and **D3** were taken and their adsorption kinetics were studied upon the addition of TBTPACOP. Analysis of the absorption spectra indicated that the hump at around 486 nm (corresponding to the absorption maxima of **D1**) has disappeared along with a minute decline in the absorption intensity of the dye **D3** (see Fig. S4, supporting information). This observation highlights the selectivity offered by TBTPACOP towards the acid dye adsorption over other dyes.

### 3. Conclusion

In conclusion, we have introduced a V-shaped Tröger's base unit to design the covalent organic polymer TBTPACOP by linking a C3-symmetric tris-amine, *N,N'*-bis(4-aminophenyl)benzene-1,4-diamine (TPA) with a C2-symmetric Tröger's base scaffold featuring dialdehyde, 4,4'-(6,12-dihydro-5,11-methanodibenzo[b,f][1,5]diazocine-2,8-diyldibenzaldehyde (TBBA), solvothermally. The synthesized polymeric material was characterised by FT-IR, solid state CP-MAS NMR and also by powder XRD, FE-SEM. The porosity of the material was further calculated by BET nitrogen adsorption-desorption analysis and the hydrophobicity of the covalent organic polymer by the contact angle measurement. The unique cleft like geometry of the Tröger's base featuring in the covalent organic polymer has resulted in structurally robust, porous polymeric material possessing hydrophobic surface and high thermal stability. The porous nature of the polymeric material has been exploited further for the dye removal from the aqueous effluent. A pseudo second order

*New. J. Chem.*

adsorption kinetics have been proposed for the dye adsorption process. It was observed that TBTPACOP has a propensity to adsorb acid dyes and can adsorb 95% of Acid Orange II from the aqueous effluent within 70 mins. The equilibrium adsorption capacity ( $q_e$ ) calculated for TBTPACOP was found to be 188.96 mg/g. Moreover, the recyclability of the COP up to four cycles, and its ability to selectively adsorb all kinds of acid dyes from the aqueous effluent in a very short time along with its high porosity, good thermal stability, high hydrophobicity makes it a promising material for the wastewater treatment and driving our mission towards the development of more sustainable materials for the future.

### Experimental Section

All chemicals were procured from Sigma-Aldrich, Spectrochem, and Avra and used directly. Silica gel-coated aluminum sheets (ACME, 254F) were used for the Thin Layer Chromatography (TLC) analysis using EtOAc and petroleum ether as the eluents. Melting points reported were uncorrected and were recorded using a capillary melting point apparatus (Thomas Hoover). Fourier-transform infrared (FT-IR) spectra were obtained with a Jasco spectrophotometer (FT-IR-4100). <sup>1</sup>H and <sup>13</sup>C NMR spectra were recorded on Bruker 400 and 500 MHz spectrometer using CDCl<sub>3</sub> and dimethyl sulfoxide-*d*<sub>6</sub> (DMSO-*d*<sub>6</sub>) as a solvent. Chemical shifts are reported in parts per million (ppm) downfield from TMS, and the spin multiplicities are described as s (singlet), d (doublet), t (triplet), dd (doublet of doublets), brs (broad singlet), and bd (broad doublet). Coupling constant (*J*) values are reported in Hertz (Hz).

The synthesis of the following compounds 2,8-dibromo-6,12-dihydro-5,11-methanodibenzo[b,f][1,5]diazocine (**2**), 2,8-dibromo-6,12-dihydro-5,11-methanodibenzo[b,f][1,5]diazocine (**3**), and tris(4-aminophenyl)amine (**6**) were performed following the reported procedure.<sup>93–94, 101–102</sup>

**Synthesis of 2,8-dibromo-6,12-dihydro-5,11-methanodibenzo[b,f][1,5]diazocine (2):**<sup>93,101</sup> 4-bromoaniline (5.0 g, 58.13 mmol) and paraformaldehyde (4.35 g, 145.3 mmol) were added to a 250 mL round-bottom flask and cooled to -15 °C. Then dropwise 50 mL of trifluoroacetic acid was added with vigorous stirring. The addition of TFA was maintained at a rate of one drop per second. After the complete addition of TFA, the flask was removed from the ice-bath and stirred for the additional 24 hours at room temperature. The red solution was then quenched slowly by pouring over 100 g of crushed ice containing 200 mL of concentrated NH<sub>4</sub>OH solution. The mixture was then extracted with 3x25 mL dichloromethane. The combined organic layers were dried over anhydrous MgSO<sub>4</sub>, filtered and concentrated to get yellow oil which was then purified by column chromatography using ethyl acetate: petroleum ether (1:9) to get hold of 2,8-dibromo-6,12-dihydro-5,11-methanodibenzo[b,f][1,5]diazocine (**2**) as pure white solid (58%); White solid, m.p. -161–165 °C; FT-IR (KBr, cm<sup>-1</sup>): 3250, 1660, 860 cm<sup>-1</sup>; <sup>1</sup>H NMR (400 MHz, CDCl<sub>3</sub>) δ 4.07 (d, *J* = 16.8 Hz, 2H), 4.22 (s, 2H), 4.61 (d, *J* = 16.8 Hz, 2H), 6.98 (d, *J* = 7.2 Hz, 2H), 7.02 (s, 2H), 7.25 (d, *J* = 7.5 Hz, 2H); <sup>13</sup>C NMR (100 MHz, CDCl<sub>3</sub>): δ 58.6, 67.0, 117.1, 127.1, 130.0, 130.0, 130.9, 147.1; HRMS (EI) Calcd for C<sub>15</sub>H<sub>12</sub>N<sub>2</sub>Br<sub>2</sub>, 377.9367; found, 377.9357.

**Synthesis of 4,4'-(6,12-dihydro-5,11-methanodibenzo[b,f][1,5]diazocine-2,8-diyldibenzaldehyde (3):**<sup>93</sup> 2,8-dibromo-6,12-dihydro-5,11-methanodibenzo[b,f][1,5]diazocine (**2**) (1.0 g, 2.63 mmol), 4-formylphenylboronic acid (1.18 g, 7.89 mmol) and the [Pd(PPh<sub>3</sub>)<sub>4</sub>](0.304 g, 0.26 mmol) were taken in a rb flask under nitrogen atmosphere and 40 mL of THF: Water (4:1) was added followed by K<sub>2</sub>CO<sub>3</sub>

(1.81 g, 13.2 mmol). The reaction mixture was refluxed for 24 h in dark. After cooling, THF was removed and the mixture was extracted with ethyl acetate, dried over  $\text{Na}_2\text{SO}_4$ , concentrated to get hold of the crude oil which was further purification by column chromatography (silica gel, ethyl acetate/pet. ether, 2:3) to yield pure compound **3** as yellow solid (78%); FT-IR (KBr,  $\text{cm}^{-1}$ ): 1710, 1600, 1120  $\text{cm}^{-1}$ ;  $^1\text{H}$  NMR (400 MHz,  $\text{CDCl}_3$ )  $\delta$  4.30-4.37 (m, 4H), 4.80 (d,  $J = 16.4$  Hz, 2H), 7.16-7.31 (m, 4H), 7.45 (s, 2H), 7.63 (s, 4H), 7.87 (s, 4H), 9.99 (d,  $J = 6.8$  Hz, 2H);  $^{13}\text{C}$  NMR (101 MHz,  $\text{CDCl}_3$ )  $\delta$  58.8, 66.8, 125.6, 125.9, 126.5, 127.2, 128.3, 130.2, 134.9, 135.5, 146.5, 148.5, 191.8; HRMS (EI) Calcd. for  $\text{C}_{29}\text{H}_{23}\text{N}_2\text{O}_2$ , 431.1759; found, 431.1765.

**Synthesis of tris(4-aminophenyl)amine (6)**<sup>94,102</sup> In a 250 ml two neck round bottom flask containing 40 mL of dry DMSO, 4-nitroaniline (a) (2.5 g, 18.1 mmol), 4-fluoro-nitrobenzene (5) (5.32 g, 4 mL, 37.7 mmol) was added followed by  $\text{K}_2\text{CO}_3$  (15 g, 108.5 mmol) were added under a positive flow of  $\text{N}_2$ . The mixture was then heated at 120 °C for 48 h and then the solvent was removed under vacuum. The formed solid was suspended in methanol and isolated by filtration. The residue was then washed successively with  $\text{H}_2\text{O}$  and methanol and dried overnight to get hold of the product tris(4-nitrophenyl)amine as yellow solid (10.3 g, 27.1 mmol) in 72% yield which was used as such for the next step.

In a 250 ml round bottom flask, suspension of tris(4-nitrophenyl)amine (5.0 g, 13.1 mmol) and 10% palladium on activated carbon (0.329 g, 3.077 mmol) in a mixture of dry 1,4-dioxane (46 mL) and EtOH (23 mL) was heated at 80 °C for 1 h under  $\text{N}_2$  atmosphere. Then hydrazine monohydrate (13 mL, 414.2 mmol) was added to the reaction mixture and the mixture was heated again at 80 °C for 48 h. On disappearance of the starting material, palladium on activated carbon was removed via vacuum filtration, the filtrate evaporated, and the crude product was crystallized at low temperature. The crystallized product was collected via vacuum filtration and dried overnight to yield 79% (3.01 g, 10.4 mmol) of tris(4-aminophenyl)amine (**6**); Gray solid, m.p: 240-242 °C; FT-IR (KBr,  $\text{cm}^{-1}$ ): 3412, 3347, 3011, 1606, 1327, 1264;  $^1\text{H}$  NMR (400 MHz,  $\text{DMSO}-d_6$ )  $\delta$  6.60-6.58 (d, 6H), 6.44-6.42 (d, 6H), 4.69 (s, 6H);  $^{13}\text{C}$  NMR (100 MHz,  $\text{DMSO}-d_6$ )  $\delta$  127.2, 114.9, 105.6; HRMS (EI) Calcd. for  $\text{C}_{18}\text{H}_{19}\text{N}_4$  ( $\text{M}^+ + \text{H}$ ) 291.16097; found, 291.1611.

**Synthesis of TBTPACOF:** To a mixture of 1:1 mesitylene/dioxane (4 mL), tris(4-aminophenyl)amine (**6**) (0.100 g, 0.344 mmol), 4,4'-(6,12-dihydro-5,11-methanodibenzo[b,f][1,5]diazocine-2,8-diyl)dibenzaldehyde (**3**) (0.222 g, 0.5166 mmol) were added followed by aqueous acetic acid solution (3 M, 0.714 mL). The reaction mixture was then degassed for 10 mins in a pyrex sealed tube (50 mL) and the tube was sealed tightly by screwing and heated at 120 °C for 3 days. The precipitate formed was collected by centrifugation, washed with THF, and dried at 120 °C under vacuum overnight to obtain TBTPACOF in 91% yield. FT-IR; 3250, 1645. 1600  $\text{cm}^{-1}$ .

#### Conflicts of Interest

The authors declare no conflicts of interest.

#### Acknowledgments

V.P.J is thankful to CSIR or the Research Fellowship. G.Y is thankful to the Swarti fellowship, Govt. of Maharashtra, India for her fellowship. The authors also acknowledges the Department of Textile Technology, ICT Mumbai for the ZEISS LSM 900 confocal laser scanning microscope facility. S.S acknowledges DST-SERB, CSIR (O2(0253)/16/EMR-II), UGC-*New. J. Chem.*

Start-Up grant (FRP (F.4-5(128)/2014(BSR), ICT Golden Jubilee research grant (2018) and CoE-PI-TEQIP-III for the financial assistance.

**Keywords:** Covalent organic polymer, Trogers base, Dye adsorption, Dye removal, Recyclable COP

- V. K. Gupta, Suhas, Application of low-cost adsorbents for dye removal—a review, *J. Environ. Manage.* 2009, **90**, 2313–2342.
- M. Rafatullah, O. Sulaiman, R. Hashim, A. Ahmad, Adsorption of methylene blue on low-cost adsorbents: a review *J. Hazard. Mater.* 2010, **177**, 70–80.
- E. N. El Qada, S. J. Allen, G. M. Walker, Adsorption of basic dyes from aqueous solution onto activated carbons, *Chem. Eng. J.* 2008, **135**, 174–184.
- R S. Blackburn, Natural Polysaccharides and Their Interactions with Dye Molecules: Applications in Effluent Treatment, *Environ. Sci. Technol.* 2004, **38**, 4905–4909.
- S. Zhuang, Y. Liu, J. Wang, Mechanistic Insight into the Adsorption of Diclofenac by MIL-100: Experiments and Theoretical Calculations, *Environ. Pollut.* 2019, **253**, 616–624.
- Y. Zhou, J. Lu, Y. Zhou, Y. Liu, Recent Advances for Dyes Removal Using Novel Adsorbents: A Review, *Environ. Pollut.* 2019, **252**, 352–365.
- Y. Zhou, M. Zhang, X. Wang, Q. Huang, Y. Min, T. Ma, J. Niu, Removal of Crystal Violet by a Novel Cellulose-Based Adsorbent: Comparison with Native Cellulose, *Ind. Eng. Chem. Res.* 2014, **53**, 5498–5506.
- S. Y. Yu, J. Mahmood, H. J. Noh, J. M. Seo, S. M. Jung, S. H. Shin, Y. K. Im, I. Y. Jeon, J. B. Baek, Direct Synthesis of a Covalent Triazine-Based Framework from Aromatic Amides, *Angew. Chemie - Int. Ed.* 2018, **57**, 8438–8442.
- G. D. Vyavahare, R. G. Gurav, P. P. Jadhav, R. R. Patil, C. B. Aware, J. P. Jadhav, Response Surface Methodology Optimization for Sorption of Malachite Green Dye on Sugarcane Bagasse Biochar and Evaluating the Residual Dye for Phyto and Cytogenotoxicity, *Chemosphere.* 2018, **194**, 306–315.
- J. M. Silva, B. S. Farias, D. D. R. Gründmann, T. R. S. Cadaval, J. M. Moura, G. L. Dotto, L. A. A. Pinto, Development of Chitosan/Spirulina Bio-Blend Films and Its Biosorption Potential for Dyes, *J. Appl. Polym. Sci.* 2017, **134**, 1–8.
- S. Roy, J. Kim, M. Kotal, R. Tabassian, K. J. Kim, I. K. Oh, Collectively Exhaustive Electrodes Based on Covalent Organic Framework and Antagonistic Co-Doping for Electroactive Ionic Artificial Muscles, *Adv. Funct. Mater.* 2019, **29**, 1–10.
- H. K. Okoro, O. S. Fatoki, F. Adekola, B. J. Kimba, R. G. Snyman, B. Opeolu, Oil Palm Biomass as an Adsorbent for Heavy Metals. *Rev., Rev. Environ. Contam. Toxicol.* 2011, **232**, 61–88.
- M. T. Chaudhry, M. Zohaib, N. Rauf, S. S. Tahir, S. Parvez, Biosorption Characteristics of *Aspergillus Fumigatus* for the Decolorization of Triphenylmethane Dye Acid Violet 49, *Appl. Microbiol. Biotechnol.* 2014, **98**, 3133–3141.
- Y. Zhuang, S. Ando, Evaluation of Free Volume and Anisotropic Chain Orientation of Tröger's Base (TB)-Based Microporous Polyimide/Copolyimide Membranes, *Polymer (Guildf).* 2017, **123**, 39–48.
- H. L. Qian, C. X. Yang, X. P. Yan, Bottom-up Synthesis of Chiral Covalent Organic Frameworks and Their Bound Capillaries for Chiral Separation, *Nat. Commun.* 2016, **7**, 12104.
- Y. H. Luo, X. T. He, D. L. Hong, C. Chen, F. H. Chen, J. Jiao, L. H. Zhai, L.

- H. Guo, B. W. Sun, Dynamic 3D Hydrogen-Bonded Organic Frameworks with Highly Water Affinity, *Adv. Funct. Mater.* 2018, **28**, 1–7.
- 17) Q. Lu, Y. Ma, H. Li, X. Guan, Y. Yusran, M. Xue, Q. Fang, Y. Yan, S. Qiu, V. Valtchev, Postsynthetic Functionalization of Three-Dimensional Covalent Organic Frameworks for Selective Extraction of Lanthanide Ions, *Angew. Chemie - Int. Ed.* 2018, **57**, 6042–6048.
- 18) G. Lin, H. Ding, R. Chen, Z. Peng, B. Wang, C. Wang, 3D Porphyrin-Based Covalent Organic Frameworks, *J. Am. Chem. Soc.* 2017, **139**, 8705–8709.
- 19) S. Mitra, H. S. Sasmal, T. Kundu, S. Kandambeth, K. Illath, D. Díaz, R. Banerjee, Targeted Drug Delivery in Covalent Organic Nanosheets (CONS) via Sequential Postsynthetic Modification, *J. Am. Chem. Soc.* 2017, **139**, 4513–4520.
- 20) P. K. Malik, Dye Removal from Wastewater Using Activated Carbon Developed from Sawdust: Adsorption Equilibrium and Kinetics, *J. Hazard. Mater.* 2004, **113**, 81–88.
- 21) G. Crini, H.N. Peindy, F. Gimbert, C. Robert, Removal of C.I. Basic Green 4 (Malachite Green) from Aqueous Solutions by Adsorption Using Cyclodextrin-Based Adsorbent: Kinetic and Equilibrium Studies, *Sep. Purif. Technol.* 2007, **53**, 97–110.
- 22) R. Malik, D.S. Ramteke, S. R. Wate, Adsorption of Malachite Green on Groundnut Shell Waste Based Powdered Activated Carbon, *Waste Manag.* 2007, **27**, 1129–1138.
- 23) B.H. Hameed, M.I. El-Khaiary, Equilibrium, Kinetics and Mechanism of Malachite Green Adsorption on Activated Carbon Prepared from Bamboo by K<sub>2</sub>CO<sub>3</sub> Activation and Subsequent Gasification with CO<sub>2</sub>, *J. Hazard. Mater.* 2008, **157**, 344–351.
- 24) O. S. Bello, M. A. Ahmad, Coconut (Cocos nucifera) Shell Based Activated Carbon for the Removal of Malachite Green Dye from Aqueous Solutions, *Sep. Sci. Technol.* 2011, **47**, 903–912.
- 25) A. Derylo-Marczewska, Analysis of the adsorption equilibrium for the system dilute aqueous solution of dissociating organic substance-activated carbon, *Langmuir.* 1993, **9**, 2344–2350.
- 26) A. R. Chowdhury, S. Maiti, A. Mondal, A. K. Das, Picolinohydrazide-Based Covalent Organic Polymer for Metal-Free Catalysis and Removal of Heavy Metals from Wastewater, *J. Phys. Chem. C* 2020, **124**, 7835–7843.
- 27) S. Maiti, A. R. Chowdhury, A. K. Das, Benzoselenadiazole-based nanoporous Covalent Organic Polymer (COP) as efficient room temperature heterogeneous catalyst for biodiesel production, *Microporous & Mesoporous Materials.* 2019, **283**, 39–47.
- 28) S. Bhowmik, R. G. Jadhav, A. K. Das, Nanoporous Conducting Covalent Organic Polymer (COP) Nanostructures as Metal-Free High Performance Visible-Light Photocatalyst for Water Treatment and Enhanced CO<sub>2</sub> Capture, *J. Phys. Chem. C* 2018, **122**, 274–284.
- 29) S. Bhowmik, M. Konda, A. K. Das, Light induced construction of porous covalent organic polymeric networks for significant enhancement of CO<sub>2</sub> gas sorption, *RSC Adv.* 2017, **7**, 47695–47703.
- 30) L. Lin, H. Guan, D. Zou, Z. Dong, Z. Liu, F. Xu, Z. Xie, Y. Li, A pharmaceutical hydrogen-bonded covalent organic polymer for enrichment of volatile iodine *RSC Adv.*, 2017, **7**, 54407–54416.
- 31) H. Uslu, G. Demir, Investigation of Efficiency of Amberlite XAD-16 on Adsorption of 2,4,6-Trinitrophenol (TNP), *Desalination. Water. Treat.* 2012, **39**, 88–94.
- 32) S. Ravi, P. Puthiaraj, K. Yu, W.-S. Ahn, Porous Covalent Organic Polymers Comprising a Phosphite Skeleton for Aqueous Nd(III) Capture *ACS Appl. Mater. Interfaces* 2019, **11**, 11488–11497.
- 33) P. R. Gogate, A. B. Pandit A Review of Imperative Technologies for Wastewater Treatment I: Oxidation Technologies at Ambient Conditions, *Adv. Environ. Res.* 2004, **8**, 501–551.
- 34) C. R. Holkar, A. J. Jadhav, D. V. Pinjari, N. M. Mahamuni, A. B. Pandit, A Critical Review on Textile Wastewater Treatments: Possible Approaches, *J. Environ. Manage.* 2016, **182**, 351–366.
- 35) H. Xu, S. Y. Ding, W. K. An, H. Wu, W. Wang, Constructing Crystalline Covalent Organic Frameworks from Chiral Building Blocks, *J. Am. Chem. Soc.* 2016, **138**, 11489–11492.
- 36) Afshari, M.; Dinari, M. Synthesis Of New Imine-Linked Covalent Organic Framework As High Efficient Adsorbent And Monitoring The Removal Of Direct Fast Scarlet 4BS Textile Dye Based On Mobile Phone Colorimetric Platform, *J. Hazard. Material.* 2020, **385**, 121514–121523.
- 37) J. Dong, F. Xu, Z. Dong, Y. Zhao, Y. Yan, H. Jin, Y. Li, Fabrication of Two Dual-Functionalized Covalent Organic Polymers through Heterostructural Mixed Linkers and Their Use as Cationic Dye Adsorbents. *RSC Adv.* 2018, **8**, 19075–19084.
- 38) S. Ravi, P. Puthiaraj, K. Yu, W. S. Ahn, Porous Covalent Organic Polymers Comprising a Phosphite Skeleton for Aqueous Nd(III) Capture, *ACS Appl. Mater. Interfaces* 2019, **11**, 11488–11497.
- 39) K. Preet, G. Gupta, M. Kotal, S. K. Kansal, D. B. Salunke, H. K. Sharma, S. C. Sahoo, P. V. D. Voort, S. Roy, Mechanochemical Synthesis of a New Triptycene-Based Imine-Linked Covalent Organic Polymer for Degradation of Organic Dye, *Cryst. Growth Des.* 2019, **19**, 2525–2530.
- 40) Y. Zhai, G. Liu, F. Jin, Y. Zhang, X. Gong, Z. Miao, J. Li, M. Zhang, Y. Cui, L. Zhang, H. Zhang, Y. Zhao, Y. Zeng, Construction of Covalent-Organic Frameworks (COFs) from Amorphous Covalent Organic Polymers via Linkage Replacement, *Angew. Chemie - Int. Ed.* 2019, **58**, 17679–17683.
- 41) P. Liu, L. Xing, H. Lin, H. Wang, Z. Zhou, Z. Su, Construction of Porous Covalent Organic Polymer as Photocatalysts for RhB Degradation under Visible Light, *Sci. Bull.* 2017, **62**, 931–937.
- 42) J. Byun, S. H. Je, H. A. Patel, A. Coskun, C. T. Yavuz, Nanoporous Covalent Organic Polymers Incorporating Tröger's Base Functionalities for Enhanced CO<sub>2</sub> Capture, *J. Mater. Chem. A.* 2014, **2**, 12507–12512.
- 43) K. S. Prakash, D.T. Masram, A reversible chromogenic covalent organic polymer for gas sensing applications, *Dalton Trans.* 2020, **49**, 1007–1010.
- 44) M. Wang, L. Guo, D. Cao, Covalent Organic Polymers for Rapid Fluorescence Imaging of Latent Fingerprints, *ACS Appl. Mater. Interfaces.* 2018, **10**, 21619–21627.
- 45) X. T. He, Y. H. Luo, D. L. Hong, F. H. Chen, Z. Y. Zheng, C. Wang, J. Y. Wang, C. Chen, B. W. Sun, Atomically Thin Nanoribbons by Exfoliation of Hydrogen-Bonded Organic Frameworks for Drug Delivery, *ACS Appl. Nano Mater.* 2019, **2**, 2437–2445.
- 46) D. Ma, Y. Wang, A. Liu, S. Li, C. Lu, C. Chen, Covalent Organic Frameworks: Promising Materials as Heterogeneous Catalysts for C-C Bond Formations, *Catalysts* 2018, **8**, 77–85.
- 47) R. Bera, M. Ansari, S. Mondal, N. Das Selective CO<sub>2</sub> capture and versatile dye adsorption using a microporous polymer with triptycene and 1,2,3-triazole motifs, *Eur. Poly. J.* 2018, **99**, 259–267.
- 48) S. Yoon, J. J. Calvo, M. C. So, Removal of Acid Orange 7 from Aqueous Solution by Metal-Organic Frameworks, *Crystals.* 2019, **9**, doi:10.3390/cryst9010017
- 49) N. Li, J. Du, D. Wu, J. Liu, N. Li, Z. Sun, G. Li, Y. Wu, Recent advances in Facile Synthesis and Applications of Covalent Organic Framework Materials as Superior Adsorbents in Sample Pretreatment, *Trends Anal. Chem.* 2018, **108**, 154–166.
- 50) X. Zhao, S. Liu, Z. Tang, H. Niu, Y. Cai, W. Meng, F. Wu, J. P. Giesy,

- Synthesis of Magnetic Metalorganic Framework (MOF) for Efficient Removal of Organic Dyes from Water, *Scientific Reports*. 2015, **5**, 11849.
- 51) Y. Zhang, S. Jin, Recent Advancements in the Synthesis of Covalent Triazine Frameworks for Energy and Environmental Applications, *Polymers*. 2019, **11**. doi:10.3390/polym11010031.
- 52) V. Mishra, V. K. Yadav, J. K. Singh, T. G. Gopakumar, Electronic Structure of a Semiconducting Imine-Covalent Organic Framework, *Chem. Asian J.* 2019, **14**, 4645–4650.
- 53) A. Mariyam, M. Shahid, I. M. M. Khan, M. Ahmad, Tetrazole Based Porous Metal Organic Framework (MOF): Topological Analysis and Dye Adsorption Properties, *J. Inorg. Organomet. P.* 2019, 1–9.
- 54) S. Luo, Q. Zhang, Y. Zhang, K. P. Weaver, W. A. Phillip, R. Guo, Facile Synthesis of a Pentiptycene-Based Highly Microporous Organic Polymer for Gas Storage and Water Treatment, *ACS Appl. Mater. Interfaces*. 2018, **10**, 15174–15182.
- 55) L. Tao, F. Niu, J. Liu, T. Wang, Q. Wang, Troger's Base Functionalized Covalent Triazine Frameworks for CO<sub>2</sub> Capture *RSC Adv.* 2016, **6**, 94365.
- 56) C. Zhang, J. Yan, Z. Tian, X. Liu, B. Cao, P. Li, Molecular Design of Tröger's Base-Based Polymers Containing Spirobichroman Structure for Gas Separation, *Ind. Eng. Chem. Res.* 2017, **56**, 12783–12788.
- 57) D. Mullangi, S. Shalini, S. Nandi, B. Choksi, R. Vaidhyanathan, Superhydrophobic Covalent Organic Frameworks for Chemical Resistant Coatings and Hydrophobic Paper and Textile Composites, *J. Mater. Chem. A*, 2017, **5**, 8376–8384.
- 58) J. L. Segur, M. J. Mancheno, F. Zamor, Covalent Organic Frameworks Based on Schiff-base Chemistry: Synthesis, Properties and Potential Applications, *Chem. Soc. Rev.* 2016, **45**, 5635–5671.
- 59) R. Mallampati, L. Xuanjun, A. Adin, S. Valiyaveetil, Fruit Peels as Efficient Renewable Adsorbents for Removal of Dissolved Heavy Metals and Dyes from Water, *ACS Sustainable Chem. Eng.* 2015, **3**, 1117–1124.
- 60) M. Samal, J. Panda, B. P. Biswal, R. Sahu, Kitchen Grinder: a Tool for the Synthesis of Metal–Organic Frameworks Towards Size Selective Dye Adsorption, *CrystEngComm*. 2018, **20**, 2486–2490.
- 61) A. A. Ahmad, B. H. Hameed, Effect of Preparation Conditions of Activated Carbon from Bamboo Waste for Real Textile Wastewater *J. Hazard. Mater.* 2010, **173**, 487–493.
- 62) E. J. Ruiz, C. Arias, E. Brillas, A. Hernández-Ramírez, J. M. Peralta-Hernández, Mineralization of Acid Yellow 36 Azo Dye by Electro-Fenton and solar Photoelectro-Fenton Processes with a Boron-doped Diamond Anode, *Chemosphere*. 2011, **82**, 495–501.
- 63) P. Puthiaraj, Y-R. Lee, S. Zhang, W-S. Ahn. Triazine-based Covalent Organic Polymers: Design, Synthesis and Applications in Heterogeneous Catalysis, *J. Mater. Chem. A*. 2016, **4**, 16288–16311.
- 64) T. Škorjanc, D. Shetty, M. A. Olson, A. Trabolsi, Design Strategies and Redox-Dependent Applications of Insoluble Viologen-Based Covalent Organic Polymers, *ACS Appl. Mater. Interfaces*. 2019, **11**, 6705–6716.
- 65) J.-H. Wang, Y. Zhang, L.-C. An, W.-H. Wang, Y.-H. Zhang, X.-H. Bu, Sulfonated Hollow Covalent Organic Polymer: Highly-Selective Adsorption toward Cationic Organic Dyes over Anionic Ones in Aqueous Solution, *Chin. J. Chem.* 2018, **36**, 826–830.
- 66) P. Song, Z. Zhang, Y. Li, P. Wang, Q. Wang, Y. Chen, Ionic Covalent Organic Polymer toward Highly Selective Removal of Anionic Organic Dyes in Aqueous Solution, 2020, *New J. Chem.* doi:10.1039/d0nj01132k
- 67) V. Sadhasivam, M. Mariyappan, A. Siva, Porous Triazine Containing Covalent Organic Polymer Supported Pd Nanoparticles: A Stable and Efficient Heterogeneous Catalyst for Sonogashira Cross-Coupling and the Reduction of Nitroarenes, *ChemistrySelect* 2018, **3**, 13442–13455.
- 68) P. Bhanja, S. K. Das, K. Bhunia, D. Pradhan, T. Hayashi, Y. Hijikata, S. Irle, A. Bhaumik, A New Porous Polymer for Highly Efficient Capacitive Energy Storage, *ACS Sus. Chem. Eng.* 2018, **6**, 202–209.
- 69) D. Dey, P. Banerjee, Toxic organic solvent adsorption by hydrophobic covalent Polymer *New J. Chem.*, 2019, DOI: 10.1039/C8NJ06249H.
- 70) B. C. Patra, S. Khilari, L. Satyanarayana, D. Pradhan, A. Bhaumik, A new benzimidazole based covalent organic polymer having high energy storage capacity, *Chem. Commun.*, 2016, **52**, 7592–7595.
- 71) B. Dolensky, M. Havlik, V. Kral, Oligo Tröger's Bases New Molecular Scaffolds, *Chem. Soc. Rev.* 2012, **41**, 3839–3858.
- 72) S. Sergeyev, Recent Developments in Synthetic Chemistry, Chiral Separations, and Applications of Tröger's Base Analogues, *Helv. Chim. Acta.* 2009, **92**, 415–444.
- 73) O. V. Rúnarsson, J. Artacho, K. Warnmark, The 125th Anniversary of the Tröger's Base Molecule: Synthesis and Applications of Troger's Base Analogues, *Eur. J. Org. Chem.* 2012, 7015–7041.
- 74) S. H. Wilen, J. Z. Qi, P. G. Williard, Asymmetric Transformation, and Configuration of Tröger's Base. Application of Tröger's Base as a Chiral Solvating Agent, *J. Org. Chem.* 1991, **56**, 485–487.
- 75) U. Maitra, B. G. Bag, First Asymmetric Synthesis of the Tröger's Base Unit on a Chiral Template, *J. Org. Chem.* 1992, **25**, 6979–6981.
- 76) M. Valík, R. M. Strongin, V. Král, Tröger's Base Derivatives-New Life for Old Compounds *Supramol. Chem.* 2005, **17**, 347–367.
- 77) J. Jensen, K. Warnmark, Synthesis of Halogen Substituted Analogues of Tröger's Base, *Synthesis*, 2001, **12**, 1873–1877.
- 78) Z-Q. Liang, X-M. Wang, Y-Y. Zhou, Z-Z. Chu, X-T. Tao, D-C. Zou, A New Pyrene Derivative Based on L-shaped Tröger's Base for Non-Doped Organic Blue Light-Emitting Diodes, *Asian J. Chem.* 2014, **26**, 1781–1785.
- 79) A. Lauber, B. Zelenay, J. Cvengros, Asymmetric Synthesis of N-stereogenic Molecules: Diastereoselective Double Aza-Michael Reaction, *Chem. Comm.* 2014, **50**, 1195–1197.
- 80) S. Shanmugaraju, D. Umadevi, A. J. Savyasachi, K. Byrne, M. Ruether, W. Schmitt, G. W. Watson, T. Gunnlaugsson, Reversible Adsorption and Storage of Secondary Explosives from Water Using a Tröger's Base-Functionalised Polymer, *J. Mater. Chem. A*. 2017, **5**, 25014–25024.
- 81) M. Carta, M. Croad, J. C. Jansen, P. Bernardo, G. Clarizia, N. B. McKeown, Synthesis of Cardo-Polymers Using Tröger's Base Formation, *Polym. Chem.* 2014, **5**, 5255–5261.
- 82) Z. Wang, D. Wang, F. Zhang, J. Jin, Tröger's base-based microporous polyimide membranes for high-performance gas separation, *ACS Macro Letters*. 2014, **3**, 597–601.
- 83) Z. Yang, R. Guo, R. Malpass-Evans, M. Carta, N. B. McKeown, M. D. Guiver, L. Wu, T. Xu, Highly Conductive Anion-Exchange Membranes from Microporous Tröger's Base Polymers, *Angew. Chem. Int. Ed.* 2016, **55**, 11499–11502.
- 84) T. V. Shishkanova, M. Havlik, V. Kral, D. Kopecky, P. Matejka, M. Dendisova, V. M. Mirsky, Amino-Substituted Tröger's Base: Electrochemical Polymerization and Characterization of the Polymer Film, *Electrochim. Acta.* 2017, **224**, 439–445.
- 85) X. Ma, M. A. Abdulhamid, I. Pinnau, Design and Synthesis of Polyimides Based on Carbocyclic Pseudo- Tröger's Base-Derived Dianhydrides for Membrane Gas Separation Applications, *Macromolecules*. 2017, **50**, 5850–5857.
- 86) Y. Zhuang, S. Ando, Evaluation of Free Volume and Anisotropic Chain Orientation of Tröger's Base (TB)-Based Microporous Polyimide/Copolyimide Membranes, *Polymer*. 2017, **123**, 39–48.

## NJC

## PAPER

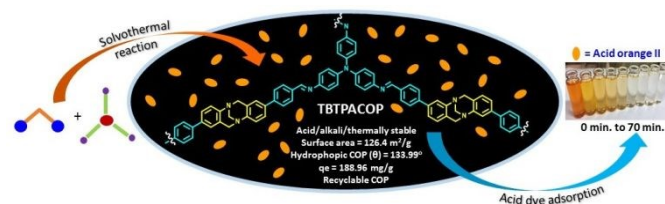
- 87) X. Ma, M. Abdulhamid, X. Miao, I. Pinnau, Facile Synthesis of a Hydroxyl-Functionalized Tröger's Base Diamine: A New Building Block for High-Performance Polyimide Gas Separation Membranes, *Macromolecules*. 2017, **50**, 9569–9576.
- 88) X. Yu, Z. Yang, H. Zhang, B. Yu, Y. Zhao, Z. Liu, G. Ji, Z. Liu, Ionic liquid/H<sub>2</sub>O-Mediated Synthesis of Mesoporous Organic Polymers and Their Application in Methylation of Amines, *Chem. Comm.* 2017, **53**, 5962–5965.
- 89) Y. Cui, Y. Liu, J. Liu, J. Du, Y. Yu, S. Wang, Z. Liang, J. Yu, Multifunctional Porous Tröger's Base Polymer with Tetraphenylethene Unit: CO<sub>2</sub> Adsorption, Luminescence and Sensing Property, *Polym. Chem.* 2017, **8**, 4842–4848.
- 90) S. Shanmugaraju, C. S. Hawes, A. J. Savyasachi, S. Blasco, J. A. Kitchen, T. Gunnlaugsson, Supramolecular Coordination Polymers Using a Close to 'V-shaped' Fluorescent 4-Amino-1,8-naphthalimide Tröger's Base Scaffold, *Chem. Comm.* 2017, **53**, 12512–12515.
- 91) S. Stehlik, T. Izak, A. Kromka, B. Dolensky, M. Havlik, B. Rezek, Sensitivity of Diamond-Capped Impedance Transducer to Tröger's Base Derivative, *ACS Appl. Mater.* 2012, **4**, 3860–3865.
- 92) D. Kim, N. M. Pugno, S. Ryu, Wetting Theory for Small Droplets on Textured Solid Surfaces, *Scientific Reports*. 2016, **6**, 37813.
- 93) A. F. M. EL-Mahdy, C. Kuo, A. Alshehri, C. Young, Y. Yamauchi, J. Kim, S. Kuo, Strategic Design of Triphenylamine- and Triphenyltriazine-Based Two-Dimensional Covalent Organic Frameworks for CO<sub>2</sub> Uptake and Energy Storage, *J. Mater. Chem. A*. 2018, **6**, 19532–19541.
- 94) J. T. Cross, N. A. Rossi, M. Serafina, K. A. Wheeler, Tröger's base quasiracemates and crystal packing tendencies, *CrystEngComm*. 2014, **16**, 7251–7258.
- 95) V. P. Jejurkar, G. Yashwantrao, B. P. K. Reddy, A. P. Ware, S. S. Pingale R. Srivastava, S. Saha, Rationally Designed Furocarbazoles as Multifunctional Aggregation Induced Emissive Luminogens for the Sensing of Trinitrophenol (TNP) and Cell-imaging, *ChemPhotoChem*, 2020, DOI: 10.1002/cptc.202000090
- 96) G. Yashwantrao, V. P. Jejurkar, R. Kshatriya, S. Saha, Solvent-Free, Mechanochemically Scalable Synthesis of 2,3-Dihydroquinazolin-4(1H)-one Using Brønsted Acid Catalyst, *ACS Sus. Chem. Eng.* 2019, **7**, 13551–13558
- 97) V. Jejurkar, C. K. Khatri, G. U. Chaturbhuj, S. Saha, Environmentally benign, highly efficient and expeditious solvent-free synthesis of trisubstituted methanes catalyzed by sulfated polyborate, *ChemistrySelect*, 2017, **2**, 11693-11696.
- 98) d spacing calculated using Bragg's law  
 $n\lambda = 2d\sin\theta$   
 Where,  $2\theta = 21^\circ$ , X-Ray wavelength = 0.15406 nm, Order of Reflection (n) = 1  
 From the Braggs law  
 $d = n\lambda/2\sin(\theta)$ ,  $d = 0.15406/2\sin(10.5)$ ,  $d = 0.42$  nm.
- 99) LSM 900 is a confocal laser scanning microscope that uses laser light in a confocal beam path to capture defined optical sections of your sample and combine them in a three-dimensional image stack. Its aperture (usually called a pinhole) is arranged in such a way that out-of-focus information will be blocked and only in-focus information can be detected. Laser module GB (pigtailed; 488, 561 nm) Diode laser (488 nm, 10 mW); laser class 3B.
- 100) Barret-Joyner-Halenda (BJH) calculation method was followed to calculate pore size distribution and it confirms the mesoporous nature of **TBTACOP**.
- 101) Lli J. Jensen, K. Wärnmark, Synthesis of Halogen Substituted Analogues of Tröger's Base, *Synthesis* 2001, **12**, 1873-1877.

*New. J. Chem.*

NJC

PAPER

Table of Contents



### Tröger's base incorporated recyclable COP for the acid dye removal from effluent.

**Abstract:** Protection of the environment from the uprising threats of pollution from several chemical industries in a sustainable way has become the major global challenge. The colored effluents from the textile and dyestuff industries are the major sources of pollution, contaminating the water bodies. Herein, we have synthesized a covalent organic polymer **TBTPACOP** having a V-shaped Tröger's base unit into the framework with the notion that the unique cleft like architecture of TB will infuse porosity and robustness in the amorphous polymeric materia. The covalent organic polymer (COP) was used for the adsorption of anionic acid dyes from the aqueous effluent. The equilibrium adsorption capacity ( $q_e$ ) was found to be 188.96 mg/g for Acid orange II. The excellent dye adsorption capacity of the COP by adsorbing 95% of Acid Orange II at room temperature within 70 mins, along with its recyclability up to 4 consecutive cycles, makes **TBTPACOP** an extremely promising material for selective and efficient removal of acid dyes from the aqueous effluent.